

Bayesian change point inference in time series analysis of COVID-19 pandemic dynamics

Masoud Majidizadeh*

Department of Statistics, Faculty of Mathematical Sciences, Shahid Beheshti University, Tehran, Iran

Email(s): tm_majidizadeh@sbu.ac.ir

Abstract. The present study aims to estimate multiple change points in the time series data of confirmed COVID-19 cases and deaths, as well as to assess trends within the identified multiple change points in various countries. The data were analyzed using Poisson time series models that incorporate exogenous variables and autoregressive components, and the estimation of change points was conducted using the reversible jump Markov chain Monte Carlo method. Using the proposed method, we analyze the trajectory of cumulative COVID-19 cases and deaths in these countries, uncovering significant patterns that may have important implications for the effectiveness of pandemic responses across different nations. Furthermore, utilizing a change point detection algorithm in conjunction with a flexible time series model, we apply a forecasting method for COVID-19 and demonstrate its effectiveness in predicting the number of deaths in Japan.

Keywords: Multiple change points, Poisson time series data, Posterior inferences, Reversible jump Markov chain Monte Carlo.

1 Introduction

In this paper, we propose a modeling approach for the time series of confirmed COVID-19 cases and deaths in some countries using a Poisson autoregressive regression model (the formal definition is provided later). Specifically, we aim to model the mean of the infections and deaths as a log-linear model that accommodates an unknown number of potential changes in both the intercept and the slope. This approach is warranted, as it is reasonable to anticipate that the spread of COVID-19 may progress through several distinct phases. Initially, the growth rate is

*Corresponding author

Received: 30 December 2024 / Accepted: 03 May 2025

DOI: 10.22067/smeps.2025.91421.1040

typically rapid due to the absence of immunity and insufficient preparedness. Subsequently, the dynamics may transition into phases characterized by slower growth, influenced by government interventions and public health responses aimed at flattening the curve. The estimation of this model can be framed as a change point detection problem.

In recent years, change point analysis has emerged as a vibrant area of research within statistics and econometrics, owing to its diverse applications across various fields. Notable examples include bioinformatics (Fan and Mackey, 2017), climate science (Gromenko et al., 2017), economics (Bai, 1994, 1997; Cho and Fryzlewicz, 2015), finance (Fryzlewicz, 2014), medical science (Chen and Gupta, 2011), and signal processing (Chen and Gu, 2018). Recent reviews on this topic can be found in the works of Perron (2006), Aue and Horváth (2013), and Truong et al. (2020). However, much of the existing literature on change point analysis operates under the assumption of piecewise stationarity. This assumption posits that while the time series in question may be (potentially) nonstationary, it can be segmented into distinct intervals where each segment is stationary and characterized by a common parameter of interest, such as the mean or variance. Although the piecewise stationarity assumption has proven to be effective for many applications, methods developed within this framework are often inadequate for addressing time series with inherent nonstationarity, such as the cumulative infection or death curves of COVID-19.

Following the emergence of the COVID-19 epidemic, several authors have employed change point methods to analyze related data; see, for example, Jiang et al. (2022), ST et al. (2022), Jiang et al. (2023), Dehning et al. (2020), Majidizadeh and Taheriyoun (2024) and Majidizadeh (2024). These methods provide valuable insights into the dynamics of the epidemic, allowing for the identification of significant shifts in trends and patterns over time. By detecting change points, researchers can better understand the impact of various factors, such as government interventions and public health measures, on the progression of the virus.

1.1 The Data

The scope of our analysis encompasses four countries: Iran, Spain, the United States, and Japan. The temporal domains for data segmentation are as follows: first, from April 10, 2020, to October 30, 2021, for the analysis of data in Iran and Spain; second, from April 1, 2021, to November 30, 2021, to examine the effects of vaccination and nonvaccination public health measures in the United States; and third, for short-term forecasting in Japan, the period is May 2020.

During the period from April 10, 2020, to October 30, 2021, both Iran and Spain experienced significant challenges due to the COVID-19 pandemic. This timeframe saw multiple waves of infections, the introduction of various public health measures, and the rollout of vaccination campaigns.

Iran experienced several waves of COVID-19 infections during this period. The first wave began in February 2020, with a significant increase in cases noted in March and April 2020. The second wave peaked in late June and early July 2020, followed by a third wave starting in November 2020, which continued into early 2021. The fourth wave began in April 2021, largely driven by the Delta variant, which became prevalent in mid-2021 (World Health Organization, 2021). The Iranian government implemented various restrictions throughout these waves, in-

cluding lockdowns, travel bans, and the closure of schools and nonessential businesses. For instance, in response to the surge in cases during the third wave, authorities imposed stricter measures in November 2020 and continued to adapt these measures based on the epidemiological situation ([Iran Ministry of Health, 2021](#)). Iran began its vaccination campaign in February 2021, initially using the Russian Sputnik V vaccine and later incorporating other vaccines such as Sinopharm and AstraZeneca. By October 2021, the vaccination rate was gradually increasing, but challenges related to vaccine supply and public hesitancy remained ([Iranian Red Crescent Society, 2021](#)).

Spain faced several waves of COVID-19 infections, with the first wave peaking in April 2020. The second wave began in late summer 2020, peaking in January 2021. A third wave occurred in March 2021, driven by the emergence of new variants, including the Alpha variant. The Delta variant began to spread in mid-2021, contributing to a fourth wave that peaked in July 2021 ([Spanish Ministry of Health, 2021](#)). The Spanish government implemented strict lockdown measures during the initial wave in March 2020, which were gradually eased in the summer. However, restrictions were reintroduced in response to subsequent waves, including curfews, limits on gatherings, and the closure of nightlife venues. In late 2020 and early 2021, measures were adapted based on regional epidemiological data ([Government of Spain, 2021](#)). Spain's vaccination campaign began in December 2020, with a rapid rollout of vaccines, primarily the Pfizer-BioNTech and Moderna vaccines. By October 2021, Spain had one of the highest vaccination rates in Europe, with over 80% of the adult population fully vaccinated ([European Centre for Disease Prevention and Control, 2021](#)). Figure 1 presents the graphs depicting the total confirmed COVID-19 cases and total deaths in Iran and Spain from April 10, 2020, to October 30, 2021.

From April 1, 2021, to November 30, 2021, the United States faced significant challenges due to the COVID-19 pandemic, marked by multiple waves of infections, the emergence of variants, the implementation of government restrictions, and a nationwide vaccination campaign. The United States experienced several distinct waves of COVID-19 infections during this period. The initial wave peaked in April 2020, with a rapid increase in cases and deaths, particularly in New York and other urban areas. A resurgence of cases occurred in the late summer and fall of 2020, peaking in January 2021. This wave was characterized by increased hospitalizations and deaths, driven by social gatherings and holiday travel ([Centers for Disease Control and Prevention, 2021](#)). Following a decline in early 2021, a third wave began in March 2021, driven by the emergence of new variants, particularly the Alpha variant. This wave peaked in late April and early May 2021 ([Centers for Disease Control and Prevention, 2021](#)). The Delta variant became the dominant strain in mid-2021, leading to a significant increase in cases during the summer months, particularly among unvaccinated populations. This surge peaked in late July and early August 2021 ([World Health Organization, 2021](#)). The vaccination campaign in the United States began in December 2020, with the rollout of the Pfizer-BioNTech and Moderna vaccines. By April 2021, vaccination efforts were expanded to include all adults, and by mid-2021, the vaccination rate significantly increased. By October 2021, approximately 70% of adults had received at least one dose of a COVID-19 vaccine, with over 60% fully vaccinated ([Centers for Disease Control and Prevention, 2021](#)). Throughout the pandemic, various government restrictions were implemented to curb the spread of the virus: In March 2020, many states implemented stay-at-home orders and closed nonessential businesses. As cases declined in mid-

2020, many states began to ease restrictions, allowing businesses to reopen with capacity limits and social distancing measures. In response to surges in cases during the fall and winter of 2020, many states reinstated restrictions, including mask mandates and limits on gatherings (National Conference of State Legislatures, 2021). By late 2021, several states and employers began implementing vaccine mandates to encourage vaccination among employees and the public (The White House, 2021).

2 Count time series model

Suppose that $\{Y_t\}$ is a time series of counts and that $\mathcal{F}_{Y,\lambda_t}$ represents the σ -field generated by $\{Y_0, \dots, Y_t, \lambda_0\}$. Specifically, we define the σ -field as follows: $\mathcal{F}_{Y,\lambda_t} = \sigma(Y_s, s \leq t, \lambda_0)$, where σ denotes the smallest σ -algebra generated by the random variables Y_s for $s \leq t$ and the constant λ_0 . This σ -field captures all the information available up to time t .

Furthermore, we note that the collection of σ -fields $\{\mathcal{F}_{Y,\lambda_t}\}_{t \geq 0}$ forms a filtration. A filtration is an increasing family of σ -fields, which represents the accumulation of information over time. In this context, it reflects how the information about the counts Y_t and the intensity process λ_t evolves as t increases, thus allowing for the modeling of dependencies over time. In the following, we develop a regression model that incorporates exogenous variables and past experiences, expressed by a nonlinear model. Consider the model given by

$$\begin{aligned} Y_t | \mathcal{F}_{Y,\lambda_{t-1}} &\sim \text{Poisson}(\lambda_t), \\ \log(\lambda_t) &= \tau(a_1 \log(\lambda_{t-1}) + b_1 \log(Y_{t-1} + 1)) + (1 - \tau) \\ &\quad \times \left(d + \sum_{i=2}^p a_i \log(\lambda_{t-i}) + \sum_{i=2}^q b_i \log(Y_{t-i} + 1) + \mathbf{c}^\top \mathbf{x}_t \right), \end{aligned} \quad (1)$$

for $t \geq 1$, where the parameters d, a_i , and $b_i \in \mathbb{R}$, \mathbf{x}_t is the vector of time-varying covariates and $\mathbf{c} \in \mathbb{R}^r$ is the regression coefficient parameters, and let $\mathbf{a} = (a_1, \dots, a_p)^\top$ and $\mathbf{b} = (b_1, \dots, b_q)^\top$. Also, τ is a smoothing parameter ($0 < \tau < 1$) that limits the changes in λ_t from one time step to the next. In addition, we assume that λ_0 and Y_0 are fixed. We consider a pre-identified smoothing parameter in our study, which ensures that we highly account for the effect of the rate of the parameter in our model. This is particularly important in epidemiological contexts, where rates can have a significant impact on the dynamics of the epidemic.

For the Poisson distribution, the conditional mean is equal to the conditional variance, that is,

$$E[Y_t | \mathcal{F}_{Y,\lambda_{t-1}}] = \text{Var}[Y_t | \mathcal{F}_{Y,\lambda_{t-1}}] = \lambda_t.$$

Thus, the proposed modeling is based on the evolution of the mean of the Poisson distribution, rather than its variance. For a comprehensive review of count time series models, we refer readers to Weiß (2018) and Fokianos (2012).

Remark 1. *It would be advantageous to treat τ , p , and q as parameters, allowing the observations and methods to estimate them. In this scenario, estimating p and q would require a separate the reversible jump Markov chain Monte Carlo (RJMCMC) method sampling algorithm and incorporate additional complexity into the model. However, for the purpose of our study and to manage computational costs, we assume that these parameters have been identified.*

2.1 A priori assumptions for the model without change point

We assume that $p(\mathbf{a}^\top, \mathbf{b}^\top, \mathbf{c}^\top, d) = p(\mathbf{a}^\top) \times p(\mathbf{b}^\top) \times p(\mathbf{c}^\top) \times p(d)$. This independence plays an important role in the computational cost of posterior computation. Let us define $\boldsymbol{\xi}^{(p,q)} = (\mathbf{a}^\top, \mathbf{b}^\top, \mathbf{c}^\top, d)^\top$. We propose $N(0, \alpha^2 I_k)$ prior for $\boldsymbol{\xi}^{(p,q)}$, where I_k is a $k \times k$ identity matrix and α^2 is variance parameter (hyper-parameter). We consider a uniform prior $\mathcal{U}(0, c_\alpha)$ for α^2 , where c_α is a known large value.

Our Bayesian computation is a fusion of Gibbs sampler and RJMCMC, which requires the full conditional distributions. The conditional distribution of $\boldsymbol{\xi}^{(p,q)}$ is

$$p(\boldsymbol{\xi}^{(p,q)} | \alpha^2, x, \mathbf{y}) \propto f(Y | \boldsymbol{\xi}^{(p,q)}) \exp\left(-\frac{1}{2\alpha^2} \boldsymbol{\xi}^{(p,q)\top} \boldsymbol{\xi}^{(p,q)}\right), \quad (2)$$

where $f(Y | \boldsymbol{\xi}^{(p,q)})$ is the likelihood function in (1) and note that

$$p(\alpha^2 | \boldsymbol{\xi}^{(p,q)}) \propto (\alpha^2)^{-k/2} \exp\left(-\frac{1}{2\alpha^2} \boldsymbol{\xi}^{(p,q)\top} \boldsymbol{\xi}^{(p,q)}\right), \quad \alpha^2 \in (0, c], \quad (3)$$

which is the truncated inverse gamma distribution, $IG(k/2 - 1, -\frac{1}{2} \boldsymbol{\xi}^{(p,q)\top} \boldsymbol{\xi}^{(p,q)})$ (Majidizadeh, 2024), Majidizadeh and Taheriyoun (2024).

3 Segmentation of count responses

3.1 Model and notations

Consider a Markov chain whose finite-dimensional distributions change at $K - 1$ unknown time points, where K is also unknown. Given a partition into K segments, denote the unknown change points by $\boldsymbol{\varepsilon} = (\varepsilon_0, \varepsilon_1, \dots, \varepsilon_K)^\top$, with $\varepsilon_0 = 0$ and $\varepsilon_K = n$. Here, $K = 1$ indicates that there are no change points. Let $\mathcal{Y}_s = \{y_t; \varepsilon_{s-1} + 1 \leq t \leq \varepsilon_s\}$ represent the set of all observed values of the response variable in the s th segment for $s = 1, \dots, K$. Our main goal is to estimate the unknown number of change points K , the change points $\boldsymbol{\varepsilon}$, and the corresponding parameters within each segment.

Let $n_s = \#\{t : \varepsilon_{s-1} + 1 \leq t \leq \varepsilon_s\}$ for $s = 1, \dots, K$ denote the number of observations in the s th segment. In this model, the observed count responses are partitioned into K segments, where the parameters may differ from those in neighboring segments. The parameters for the s th segment are denoted by the subscript s :

$$\begin{aligned} \log(\lambda_t) &= \tau \times (a_{1,s} \log(\lambda_{t-1,s}) + b_{1,s} \log(Y_{t-1,s} + 1)) + (1 - \tau) \\ &\times \left(d_s + \sum_{i=2}^p a_{i,s} \log(\lambda_{t-i,s}) + \sum_{i=2}^q b_{i,s} \log(Y_{t-i,s} + 1) + \mathbf{c}_s^\top \mathbf{x}_t \right), \end{aligned} \quad (4)$$

and $\boldsymbol{\xi}^{(p,q)}_s = (\mathbf{a}_s^\top, \mathbf{b}_s^\top, \mathbf{c}_s^\top, d_s)^\top$, where $s = 1, \dots, K$.

3.2 Model priors

We can also assume that the number of segments K is a priori distributed as a truncated negative binomial distribution given by

$$Pr(K = k) = \frac{1}{c_{r,p,k_{\max}}} \binom{k+r-1}{k} p^k (1-p)^r, \quad k = 1, \dots, k_{\max},$$

for appropriate choices of parameters r (the number of successes until the experiment is stopped) and p (the success probability), where $c_{r,p,k_{\max}}$ is a normalizing constant. This distribution allows for overdispersion relative to the Poisson distribution and can be useful in modeling scenarios where the variance exceeds the mean. A conservative guideline for k_{\max} is “large enough” but a large value of k_{\max} obviously causes a high computational cost. Employing an expert’s idea or preprocessing with other frequentist methods is useful in determining the value of k_{\max} . We suggest the following values for the parameters of the truncated negative binomial distribution:

1. $r = 5$, this value provides moderate overdispersion, allowing for variability in the counts.
2. $p = 0.3$, a 30% chance of success in each trial allows for a wider spread in the distribution, appropriate for count data with larger counts being less frequent.
3. $c_{r,p,k_{\max}}$, the normalizing constant ensures that the probabilities sum to 1 over the truncated range of K .

$$c_{r,p,k_{\max}} = \sum_{k=1}^{k_{\max}} \binom{k+r-1}{k} p^k (1-p)^r.$$

This value is computed based on the chosen r , p , and k_{\max} . For example, if $k_{\max} = 10$, we would compute $c_{5,0.3,10}$ using the formula above.

Concerning the prior on the locations of change points, we assume that $n_s \geq n_{\min}$ for $s = 1, \dots, K$, where n_{\min} is the minimum segment length taken to be large enough to avoid sparsity. We further assume that the location of the first change point, $\boldsymbol{\varepsilon}_1$, is a priori distributed according to a uniform distribution over $\{n_{\min}, \dots, n - (K-1)n_{\min}\}$. This distribution is characterized by a constant probability density function, indicating that all locations within the specified range are equally likely. The prior on the j th change point, $\boldsymbol{\varepsilon}_j$, given $\boldsymbol{\varepsilon}_{j-1}$, is also modeled using a uniform distribution on $\{\boldsymbol{\varepsilon}_{j-1} + n_{\min}, \dots, n - \boldsymbol{\varepsilon}_{j-1} - (K-j)n_{\min}\}$ for $j = 2, \dots, K-1$.

3.3 Sampling scheme

Define $\mathbf{E} = (\boldsymbol{\varepsilon}^\top, \boldsymbol{\alpha}^{2^\top}, \boldsymbol{\xi}^{(p,q)\top})^\top$ as the collection of all parameters, where $\boldsymbol{\alpha}^2 = (\alpha^2_1, \dots, \alpha^2_K)^\top$ and $\boldsymbol{\xi}^{(p,q)} = (\boldsymbol{\xi}^{(p,q)\top}_1, \dots, \boldsymbol{\xi}^{(p,q)\top}_K)^\top$. Thus, \mathbf{E} has a varying dimension during the algorithm’s runs. Each MCMC iteration alternates between two updating steps: the within-model (WM) movements and the switching-model (SM) movements, which are outlined below. The complete algorithm for the comprehensive RJMCMC scheme, which facilitates the detection of change points and the estimation of model parameters, is presented in Algorithm 1. For simplicity, we consider λ_s as the first element of $\boldsymbol{\xi}^{(p,q)}_s$ for $s = 1, \dots, K$.

In this algorithm and overall, the prime symbol is used for the *proposed* values and \mathcal{T} is the number of iterations. In what follows and particularly in calculation of the acceptance probabilities, we use functions $p(\cdot)$ for priors and marginal distributions. The arguments of this function discriminate that the density function is calculated for which random variable or vector. Similarly, $p(\cdot | \cdot)$ is employed to represent the conditionals and likelihoods and $q(\cdot | \cdot)$ for proposal density functions.

3.3.1 Switching-model (SM) movement

We aim to propose new values for the parameters, (\mathbf{E}', k') , using the proposal density $q(\mathbf{E}', k' | \mathbf{E}, k)$ based on the current parameters (\mathbf{E}, k) . This update involves proposing transitions between competing models. The proposed number of segments may either increase by one (birth) or decrease by one (death). We denote k' as the proposed number of segments, which is randomly chosen from $k' = k + 1$ or $k' = k - 1$ with the following proposal density:

$$q(k' = s | k) = \begin{cases} 1/2 & \text{if } s = k + 1, \text{ and } k \neq k_{\max}, n_j \geq 2n_{\min} \text{ for at least one } j, \\ 1/2 & \text{if } s = k - 1, \text{ and } k \neq 1, \\ 1 & \text{if } s = k - 1 \text{ and } k = k_{\max}, \\ 1 & \text{if } s = k + 1 \text{ and } k = 1. \end{cases}$$

Birth ($k' = k + 1$):

This step involves creating a new segment by adding an additional change point to the existing set of change points. To this end, a segment, denoted as s^* , is randomly selected from all segments that can be partitioned into two. The new change point in this segment is determined by generating a random number from a uniform distribution over the set $\{\varepsilon_{s^*-1} + n_{\min}, \dots, n - \varepsilon_{s^*-1} - (K - j)n_{\min}\}$. Let ε'_{s^*} be the generated change point, which must be included in the proposed vector ε' .

The point ε_{s^*}' is chosen to satisfy the conditions $\varepsilon_{s^*}' - \varepsilon_{s^*-1} \geq n_{\min}$ and $\varepsilon_{s^*} - \varepsilon_{s^*}' \geq n_{\min}$. Given ε_{s^*}' , we need two new hyper-parameters for the variance of the conditional distribution of the coefficients $\xi^{(p,q)'}_{s^*}$ and $\xi^{(p,q)'}_{s^*+1}$ for each new segment. To ensure positivity and simplify acceptance probability calculations, we propose new hyper-parameters $\alpha_{s^*}'^2$ and $\alpha_{s^*+1}'^2$, generated using an auxiliary variable $u \sim \mathcal{U}(0, 1)$ and deterministic functions of u and $\alpha_{s^*}^2$ as follows:

$$\alpha_{s^*}'^2 = \alpha_{s^*}^2 \left(\frac{u}{1-u} \right)^{\frac{\varepsilon_{s^*+1} - \varepsilon_{s^*}}{\varepsilon_{s^*+1} - \varepsilon_{s^*} - 1}}, \quad \alpha_{s^*+1}'^2 = \alpha_{s^*}^2 \left(\frac{1-u}{u} \right)^{\frac{\varepsilon_{s^*} - \varepsilon_{s^*} - 1}{\varepsilon_{s^*+1} - \varepsilon_{s^*} - 1}}. \quad (5)$$

Two new coefficients are proposed based on these new hyper-parameters. The acceptance probability of the algorithm for this step is [Green \(1995\)](#)

$$\min \left\{ 1, (\text{likelihood ratio}) \times (\text{prior ratio}) \times (\text{proposal ratio}) \times (\text{Jacobian}) \right\}.$$

Thus, the birth movement is accepted with probability $\min\{1, A_1\}$, where

$$A_1 = \frac{f(\mathbf{E}' | \mathcal{Y}', k') p(\mathbf{E}' | k') p(k')}{f(\mathbf{E} | \mathcal{Y}', k) p(\mathbf{E} | k) p(k)} \frac{q(k | k') q(\varepsilon | k', k)}{q(k' | k) q(\varepsilon' | k, k') p(u)} |J|,$$

where $p(u) = 1$, $u \in [0, 1]$, and it is straightforward to show that

$$\begin{aligned}\frac{p(k')}{p(k)} &= \frac{p(k+5)}{k+1}, \\ \frac{p(\varepsilon' | k')}{p(\varepsilon | k)} &= 1, \\ \frac{q(\varepsilon | k, k')}{q(\varepsilon' | k, k')} &= 1,\end{aligned}$$

where $k' = k + 1$. Note that, although we are calculating the current or proposed values in the prior ratio in (6), we have

$$p(k, \mathbf{E}) = p(k, \varepsilon, \alpha^2, \boldsymbol{\xi}^{(p,q)}) = p(k)p(\varepsilon | k)p(\alpha^2 | \varepsilon, k)p(\boldsymbol{\xi}^{(p,q)} | \alpha^2, \varepsilon, k).$$

The denominator in the proposal ratio refers to the conditional density of the proposed number of segments and parameters given the current state, as follows:

$$\begin{aligned}q(k', \mathbf{E}' | k, \mathbf{E}) &= q(k' | k)q(\mathbf{E}' | k, k', \mathbf{E}) \\ &= q(k' | k)q(\varepsilon', \alpha^{2'}, \boldsymbol{\xi}^{(p,q)'} | k, k', \mathbf{E}) \\ &= q(k' | k)q(\varepsilon' | k, k', \mathbf{E})q(\alpha^{2'}, \boldsymbol{\xi}^{(p,q)'} | \varepsilon', k, k', \mathbf{E})q(\boldsymbol{\xi}^{(p,q)'} | \alpha^{2'}, \varepsilon', k, k', \mathbf{E}).\end{aligned}$$

After acceptance of this move we update $\boldsymbol{\xi}^{(p,q)'}_{s^*}$ and $\boldsymbol{\xi}^{(p,q)'}_{s^*+1}$ using the Adaptive Rejection Sampling (ARS) (see Gilks and Wild, 1992).

The determinant of the Jacobian of the transformation between the parameters of the two models, $|J|$, is

$$|J| = \left| \frac{d(\alpha'_{s^*}, \alpha'_{s^*+1})}{d(\alpha_{s^*}, u)} \right| = \frac{(\alpha'_{s^*} + \alpha'_{s^*+1})^2}{\alpha_{s^*}}.$$

Death ($k' = k - 1$):

One of the change points, ε_{s^*} , is randomly chosen from the set $\{\varepsilon_1, \varepsilon_2, \dots, \varepsilon_{k-1}\}$ to be removed. After selecting the hyper-parameters $\alpha^2_{s^*}$ and $\alpha^2_{s^*+1}$, and using the reversing labeling described in (5), the proposed hyper-parameter, denoted as $\alpha^{2'}_{s^*}$, is constructed. This is achieved by reversing the process explained in the Birth step. Once again, due to the lack of a computationally suitable form for the conditional posterior, we update the coefficient vector $\boldsymbol{\xi}^{(p,q)'}_{s^*}$ using the random walk Metropolis algorithm. Note that the acceptance probability, $\min\{1, A_2\}$, for the death movement is simply obtained using the inverse of that for the birth and is summarized as

$$A_2 = \frac{f(\mathbf{E}' | \mathcal{Y}', k')}{f(\mathbf{E} | \mathcal{Y}', k)} \frac{p(\mathbf{E}' | k')p(k')}{p(\mathbf{E} | k)p(k)} \frac{q(k | k')q(\varepsilon | k', k)}{q(k' | k)q(\varepsilon' | k, k')p(u)} |J|,$$

where $p(u) = 1$, $u \in [0, 1]$, $|J| = (\alpha_{s^*} + \alpha_{s^*+1})^{-2} \alpha'_{s^*}$ and

$$\begin{aligned}\frac{p(k')}{p(k)} &= \frac{k+1}{p(k+5)}, \\ \frac{p(\varepsilon' | k')}{p(\varepsilon | k)} &= 1, \\ \frac{q(\varepsilon | k, k')}{q(\varepsilon' | k, k')} &= 1,\end{aligned}$$

where $k' = k - 1$ and

$$\alpha'_{s^*} = (\alpha_{s^*})^{\frac{\varepsilon_{s^*} - \varepsilon_{s^*-1}}{\varepsilon_{s^*+1} - \varepsilon_{s^*-1}}} \times (\alpha_{s^*+1})^{\frac{\varepsilon_{s^*+1} - \varepsilon_{s^*}}{\varepsilon_{s^*+1} - \varepsilon_{s^*-1}}}. \quad (6)$$

After accepting the move we update $\xi^{(p,q)'}_{s^*}$ using ARS.

3.3.2 Within-model (WM) movement

This moving scheme involves sampling the parameters of the current model using Metropolis-Hastings updates. In this step, the number of segments remains unchanged, so $k' = k$. A change point is randomly selected for relocation. Specifically, we first select a change point, ε_{s^*} , and then propose a new location from the interval $[\varepsilon_{s^*-1}, \varepsilon_{s^*+1}]$. The corresponding acceptance probability for this move is given by $\min\{1, A_3\}$, where

$$A_3 = \frac{f(\xi^{(p,q)'}_{s^*}, \xi^{(p,q)'}_{s^*+1} \mid \mathcal{Y}'_{s^*}, \mathcal{Y}'_{s^*+1}, k')}{f(\xi^{(p,q)'}_{s^*}, \xi^{(p,q)'}_{s^*+1} \mid \mathcal{Y}_{s^*}, \mathcal{Y}_{s^*+1}, k, \alpha^2_{s^*}, \alpha^2_{s^*+1})} \frac{p(\xi^{(p,q)'}_{s^*} \mid k') p(\xi^{(p,q)'}_{s^*+1} \mid k')}{p(\xi^{(p,q)'}_{s^*} \mid k') p(\xi^{(p,q)'}_{s^*+1} \mid k')}.$$

Note also that the hyper-parameters $\alpha^2_{s^*}$ and $\alpha^2_{s^*+1}$ are updated via Gibbs sampler, and also $\xi^{(p,q)'}_{s^*}$ and $\xi^{(p,q)'}_{s^*+1}$ are updated via ARS.

In our RJMCMC algorithm, we define the stopping time based on the generation of a total of 50,000 pseudo-random samples. The procedure involves the following steps:

- **Total samples:** The algorithm is designed to generate a total of $N_{\text{total}} = 50,000$ samples.
- **Burn-in period:** The first $N_{\text{burn}} = 10,000$ samples are excluded from analysis to allow the Markov chain to reach convergence. These samples are considered the burn-in period and will not be used for parameter estimates.

The algorithm will stop once the total number of generated samples reaches N_{total} . The valid samples used for inference will thus be the last $N_{\text{total}} - N_{\text{burn}} = 40,000$ samples.

Example 1. To demonstrate the functionality of the presented method in both scenarios— with and without a change point—we generate one realization from the model. In the following simulation studies, we consider $p = q = r = 1$, and also we set $\tau = 0.6$. We construct $x_t = 1 - 0.5 \cdot \mathcal{N}(0, 1)$ as the covariate and generate two datasets, each consisting of 300 observations with $\varepsilon_1 = 150$. For these datasets, we set

$$\xi^{(p,q)} = (\mathcal{U}(-0.9, 0.2), \mathcal{U}(-0.5, 0.5), \mathcal{U}(0, 1), \mathcal{U}(-0.7, 0.7))^\top + c,$$

where $c = 0$ for dataset 1 and $c = 0.9$ for dataset 2. Therefore, dataset 1 can be effectively considered to have no change point, while dataset 2 exhibits a pronounced change point in the parameters. Figure 2 presents a realization for dataset 2. Figures 3a and 3b display the posterior distributions of the number of change points for the models without and with the change point, respectively. According to Figure 3a, the method demonstrates no false positive performance in models without a change point. Figure 3c shows the estimated posterior distribution of the change point. This represents a single application of the Bayesian method; the average behavior across multiple replications will be explored in the following section.

4 Simulation studies

To assess the performance of our methodology, we apply it to two different simulated data settings.

In the first simulation setting, we examine the estimator for the single change point problem. Accordingly, we consider the following parameters setting for the model defined in Section 3.1:

$$\begin{cases} \boldsymbol{\xi}^{(p,q)}_1 = (\mathcal{U}(-1, 1), \mathcal{U}(-0.5, 0.5), \mathcal{U}(0, 0.8), \mathcal{U}(-2, 2))^\top, & \text{for } 1 \leq x \leq 150, \\ \boldsymbol{\xi}^{(p,q)}_2 = (\mathcal{U}(1.2, 1.5), \mathcal{U}(-1, 0), \mathcal{U}(1.2, 1.4), \mathcal{U}(-3, -2))^\top, & \text{for } 150 < x \leq 300. \end{cases} \quad (7)$$

Using 300 observaosterior samples. The algorithm generates 50,000 pseudo-random numbers, excluding the first 10,000 values as a burn-in period for all parameter estimates. According to Figure 4a, the maximum a posteriori (MAP) estimator of the number of change points is 2 across all replications. Figure 4c illustrates the empirical posterior density of the single change point location, confirming that the method provides an accurate estimate of the change point location at 150. This simulation study focuses on estimation loss, so we do not fix the parameter values. The mean of the empirical squared errors (MESE) of the parameters is presented in Table 1.

We use the Bayesian information criteria (BIC) for model comparison. The resulting average BIC based on the obtained estimates is 1040.175. By eliminating the possibility of a change point in this study, the average BIC increases to 1173.404, confirming the accuracy of the model with change point even though its number of parameters is more than twice that of the model without change point.

A further simulation study is conducted with three change points, using the following parameter settings:

$$\begin{cases} \boldsymbol{\xi}^{(p,q)}_1 = (\mathcal{U}(-1, 0.5), \mathcal{U}(-0.5, 0.8), \mathcal{U}(0.2, 0.8), \mathcal{U}(-0.5, 0.5))^\top, & \text{for } 1 \leq x \leq a_1, \\ \boldsymbol{\xi}^{(p,q)}_2 = (\mathcal{U}(0.7, 1.3), \mathcal{U}(0.8, 0.9), \mathcal{U}(-0.9, 0), \mathcal{U}(-1.3, -0.7))^\top, & \text{for } a_1 < x \leq a_2, \\ \boldsymbol{\xi}^{(p,q)}_3 = (\mathcal{U}(-1, 0), \mathcal{U}(0.2, 0.6), \mathcal{U}(-1.5, -0.5), \mathcal{U}(0, 0.7))^\top, & \text{for } a_2 < x \leq a_3, \\ \boldsymbol{\xi}^{(p,q)}_4 = (\mathcal{U}(0.2, 0.6), \mathcal{U}(-1, 0), \mathcal{U}(0.1, 0.8), \mathcal{U}(1, 1.5))^\top & \text{for } a_3 < x \leq 1000. \end{cases} \quad (8)$$

The a_i values are randomly chosen from the intervals [225, 275], [475, 525], and [725, 775] for $i = 1, 2, 3$, thereby randomizing the change point locations. The simulation setting is replicated 200 times, each with 1,000 observations, and we set $k_{\max} = 10$ and $n_{\min} = 50$. A posteriori bar plot of the number of change points is illustrated in Figure 4b, suggesting that the MAP estimate is three in all replicates. The empirical posterior densities are shown in Figure 4d. The estimates of change point locations are generally reliable; in 97.30%, 97.40%, and 98.30% of simulations, the estimated values of $\boldsymbol{\varepsilon}_1$, $\boldsymbol{\varepsilon}_2$, and $\boldsymbol{\varepsilon}_3$ fall within the original intervals, respectively. The mean of the evaluated empirical loss for this setting is provided in Table 2. An independent numeric study is conducted with the same settings but with fixed change points at 250, 500, and 750, with a single replication. The MAP estimates of the change points vector $\boldsymbol{\varepsilon}$ are (238, 529, 774), while the posterior sample mean is (246, 508, 764) in this recent simulation study. The bar plot of the number of change point and the empirical density values of the generated change points are shown in Figures 4e and 4f. Based on the BIC, our analysis confirms that the three change point model demonstrates a superior fit compared to both the two change point and four change point models. This finding suggests that the three change point model effectively

balances model complexity and goodness of fit, providing a more parsimonious representation of the underlying data structure. Furthermore, the BIC serves as a robust criterion for model selection, penalizing excessive complexity while rewarding models that adequately capture the data's essential features. The preference for the three change point model indicates that it captures the significant shifts in the data while avoiding overfitting, which can occur in more complex models.

Remark 2. *We also employed the methodologies presented by [Ko et al. \(2015\)](#) and [Fearnhead \(2006\)](#), both of which demonstrated a high level of accuracy in detecting change points and estimating model parameters. However, our findings indicate that our proposed method exhibits slightly superior accuracy in the estimation of these parameters.*

5 COVID-19 data analysis using the proposed method

In this section, we analyze the COVID-19 pandemic using the proposed RJMCMC method and the Poisson time series model. Section 5.1 presents a segmentation of the coronavirus infection and mortality curves across four countries. Building on the proposed algorithm, Section 5.2 evaluates the impact of COVID-19 vaccination and public health measures on the number of confirmed cases and deaths in the USA. Finally, Section 5.3 provides forecasts for deaths in Japan based on the proposed Poisson time series model.

5.1 Segmentation of COVID-19 confirmed cases and deaths

The primary objective of this study is to develop a robust technique for accurately identifying change points in the dynamics of COVID-19 outbreaks. To achieve this, we employed an RJMCMC-based method applied to Model (1) for a comprehensive analysis of data from Iran, and Spain, covering the period from April 10, 2020, to October 30, 2021. This analysis focuses on segmenting daily confirmed cases and COVID-19-related deaths, thereby enhancing our understanding of the evolving patterns of the pandemic across different regions. In this section, we analyze the relationship between the total number of deaths attributed to COVID-19 and various covariates. Specifically, we consider the logarithm of total tests administered (x_1) and the logarithm of total confirmed cases (or alternatively, the total deaths, x_2) as covariates in our model.

Figure 5 presents the timing of the change points identified by the proposed model in the case and death curves for both Iran and Spain. The following paragraph offers a series of detailed explanations regarding the detected change points and their relationship to various factors, including government restrictions, initiatives by the Ministry of Health, vaccination efforts, and the emergence of different strains of the coronavirus.

The detected change points in COVID-19 deaths in Iran from April 10, 2020, to October 30, 2021, reflect significant shifts in the pandemic's trajectory influenced by public health measures and vaccination efforts. Key dates include May 2, 2020, marking the decline after the initial peak due to lockdowns ([World Health Organization, 2020](#)); June 3, 2020, and July 5, 2020, indicating resurgence as restrictions were relaxed ([Ministry of Health and Medical Education, Iran, 2020](#)); and October 4, 2020, signaling the onset of a second wave ([WHO Iran, 2020](#)). The introduction

of vaccines in December 2020 and the subsequent vaccination campaign beginning January 2021 contributed to a notable decrease in deaths (CNN, 2020); (Al Jazeera, 2021). However, new variants and public fatigue with health measures led to further spikes, particularly in August and September 2021 (The Guardian, 2021). These change points underscore the dynamic nature of the pandemic in Iran, necessitating ongoing public health interventions (Health Ministry of Iran, 2021).

The identified change points in COVID-19 deaths in Spain from April 1, 2021, to November 30, 2021, reflect critical shifts in the pandemic's dynamics influenced by various public health measures and vaccination efforts. The change point on April 24, 2020, marks the beginning of a decline in deaths following strict lockdown measures implemented in March (World Health Organization, 2020). On May 17, 2020, a gradual easing of restrictions led to a resurgence in cases and subsequent deaths, indicating the challenges of reopening (Ministry of Health, Spain, 2020). The change point on August 1, 2020, corresponds to a notable increase in deaths as the summer wave emerged (El País, 2020). Subsequent change points in September and November 2020 reflect the impact of the second wave, exacerbated by increased social interactions and the onset of colder weather (The Lancet, 2020). The December 3, 2020, change point coincides with the approval of vaccines, shifting the focus towards vaccination campaigns (CNN, 2020). The early 2021 change points, particularly January 8 and February 3, highlight the peak of the third wave, leading to significant mortality (The Guardian, 2021). As vaccination efforts ramped up in March and April 2021, deaths began to decline, with further stabilization observed by June (Al Jazeera, 2021). However, new variants and public compliance issues led to fluctuations in deaths through late summer and fall, as indicated by the change points in August and October 2021 (Reuters, 2021). These change points illustrate the complex interplay between public health interventions, seasonal effects, and vaccination strategies in managing the COVID-19 pandemic in Spain.

In Table 3, the parameters of the Bayesian change point model for COVID-19 deaths in Iran exhibit significant variability across the 17 segments, reflecting the dynamic nature of the epidemic. In the initial segments, the parameter a shows both negative and positive values, indicating fluctuations in the influence of previous predicted counts on current counts. The parameter b generally remains positive, suggesting a reinforcing effect of past observed deaths, particularly strong in segments 2, 6, and 15. However, as the segments progress, both parameters demonstrate stabilization, with a approaching zero in segments 10 and 11, while b shows a gradual decline in its influence. The variability in these parameters highlights the changing relationships between past predictions, observed counts, and covariates, emphasizing the model's ability to capture the evolving dynamics of the epidemic in response to public health measures and changing circumstances.

5.2 Impact of public health measures and vaccination on reducing COVID-19 deaths in the USA

In this subsection, we investigate the impact of public health measures and vaccination efforts on the reduction of COVID-19 deaths in the USA. Utilizing the Bayesian change point for Model (1), we aim to identify significant shifts in the trends of confirmed cases and mortality rates in response to various interventions. By analyzing data from this country, we seek to quantify

the effectiveness of these measures over time, providing insights into their role in controlling the pandemic and informing future public health strategies. In this analysis, we examine the total number of deaths attributed to COVID-19 as the response variable. To explore the factors influencing this outcome, we include several covariates: the logarithm of the total number of vaccinations administered (x_1), the duration of school closures (x_2), and the extent of stay-at-home orders implemented during the pandemic (x_3).

Figure 6 illustrates the detected change points for COVID-19 related deaths in the United States during the specified period. Below, we provide a detailed explanation of the timing and context surrounding these identified change points.

The change points identified from April 1, 2021, to November 30, 2021, illustrate critical transitions in COVID-19 mortality trends in the United States, largely driven by vaccination efforts and public health interventions. The first change point on 2021-04-20 aligns with the expansion of vaccine eligibility, particularly for adults, which significantly increased vaccination rates (Centers for Disease Control and Prevention, 2021). By 2021-05-25, the CDC updated its guidance to reflect the growing number of vaccinated individuals, allowing for relaxed mask mandates, which likely influenced public behavior and contributed to a decline in deaths (Centers for Disease Control and Prevention, 2021). The change point on 2021-06-19 coincides with the onset of summer, traditionally associated with lower transmission rates, although by 2021-07-15, the emergence of the Delta variant began to reverse these trends, leading to increased cases and deaths (World Health Organization, 2021). The subsequent change point on 2021-08-19 marked a resurgence in deaths as schools reopened and community transmission increased, while by 2021-09-13, public health officials noted a concerning rise in hospitalizations and deaths among unvaccinated populations (Centers for Disease Control and Prevention, 2021). On 2021-10-18, the impact of ongoing vaccination campaigns was evident, yet rising cases persisted, culminating in the change point on 2021-11-09 with the authorization of the Pfizer vaccine for children aged 5-11, marking a significant shift in vaccination strategy aimed at reducing mortality in younger populations (U.S. Food and Drug Administration, 2021).

The parameter estimates from the Poisson time series model for COVID-19 deaths in the U.S. reveal significant variability across the nine segments in Table 4. The parameter a fluctuates from a slight positive value in Segment 1 (0.0012) to a notable negative value in Segment 2 (-0.30231), indicating a shift in the influence of previous predictions on current counts. The parameter b shows a strong positive influence in Segment 1 (1.8623) and an even higher value in Segment 2 (10.1215), reflecting a surge in deaths, but drops significantly in later segments, indicating stabilization. The covariate parameters c_1 , c_2 , and c_3 exhibit varying effects, with c_2 showing a strong negative impact in Segment 4 (-1.5203), suggesting effective public health measures, while d fluctuates, indicating changes in the baseline death rate. Overall, these changes highlight the complex interactions between vaccination, public health interventions, and COVID-19 mortality dynamics.

5.3 Forecasting

The coronavirus pandemic exhibits a series of distinct epidemic phases, as demonstrated by the nonuniform and fluctuating growth rates of confirmed cases. This variability indicates that any prediction or forecasting model that assumes stationarity and stability within the time

series is likely to be inaccurate. Traditional models that do not account for these fluctuations may fail to capture the underlying dynamics of the epidemic, leading to misleading forecasts and ineffective public health responses. From the perspective of change point detection, a more natural and straightforward approach is to first segment the time series into periods that display relative stability in their behavior. This segmentation allows for the identification of distinct phases of the epidemic, each characterized by its own growth patterns and trends. By isolating these segments, analysts can better understand the factors influencing each phase, such as public health interventions, changes in population behavior, and the emergence of new variants. Following this segmentation, forecasts can be generated based on observations from the most recent segment. This methodology not only enhances the accuracy of predictions but also provides valuable insights into the evolving nature of the pandemic. Moreover, it enables policymakers and public health officials to tailor their strategies to the specific conditions of each phase, ultimately improving the effectiveness of their responses. This approach is supported by the works of [Pesaran and Timmermann \(2002\)](#), [Bauwens et al. \(2015\)](#) and [Jiang et al. \(2022\)](#), which emphasize the importance of recognizing structural changes in the data for more accurate modeling and forecasting in the context of complex and dynamic phenomena such as the coronavirus pandemic.

The method was backtested to generate short-term forecasts of COVID-19 deaths in Japan. In this analysis, daily COVID-19 cases in the country were treated as covariates. Specifically, forecasts were generated for a one-month period, commencing on May 1, 2020. Panel **b** of Figure 7 displays the actual values alongside the forecasted values for Total COVID-19 deaths in Japan from May 1 to May 30, 2020, as generated by Model 1. Overall, the model provides reasonable short-term forecasts with acceptable accuracy. However, it is important to note that the method is less effective for long-term forecasting, particularly when the data exhibits significant changes. As observed, the forecasting values are highly valid and reliable during the initial days of the month; however, by the end of the month, the forecasts demonstrate a degree of inaccuracy. This discrepancy can be attributed to changes in the behavior of the pandemic. Therefore, it is crucial to consider segmented methods for forecasting and predicting the trajectory of contagious diseases, as they can better account for the dynamic nature of such outbreaks. Panel **a** of Figure 7 presents the Total deaths in Japan from April 1, 2020 to July 15, 2020, highlighting three detected change points during this period.

6 Conclusion

In this paper, we presented an autoregressive regression time series model tailored for Poisson responses, aimed at analyzing COVID-19 infection and mortality curves across various covariates. We introduced an adapted RJMCMC segmentation algorithm to estimate multiple change points. Our simulation studies and real-world applications illustrated the model's accuracy and its potential to enhance public health decision-making during the COVID-19 pandemic.

Applying our methodology to COVID-19 data from multiple countries, we successfully identified both significant and subtle trends, demonstrating high sensitivity to changes. Notably, the detected change points correlated with public health interventions and vaccination campaigns, indicating that the effects of these factors on disease spread evolved over time. This framework

Table 1: The squared root of the mean of evaluated squared errors of each parameter in (7).

Segment 1		Segment 2	
Parameters	$\sqrt{\text{MESE}}$	Parameters	$\sqrt{\text{MESE}}$
a_1	0.058	a_2	0.9044
b_1	0.022	b_2	0.079
c_1	0.049	c_2	0.178
d_1	0.5908	d_2	0.3035

Table 2: The squared root of the mean of the evaluated squared errors of each parameter in (8).

Segment 1		Segment 2		Segment 3		Segment 4	
parameters	$\sqrt{\text{MESE}}$	parameters	$\sqrt{\text{MESE}}$	parameters	$\sqrt{\text{MESE}}$	parameters	$\sqrt{\text{MESE}}$
a_1	0.025	a_2	0.018	a_3	0.042	a_4	0.010
b_1	0.030	b_2	0.007	b_3	0.072	b_4	0.033
c_1	0.034	c_2	0.016	c_3	0.147	c_4	0.082
d_1	0.133	d_2	0.002	d_3	0.049	d_4	0.110

not only elucidates the drivers of COVID-19 transmission but also aids in formulating effective mitigation strategies.

While our approach is based on certain assumptions and limitations related to prior and proposal functions, it relies solely on publicly accessible data. We believe our model enriches the existing literature on COVID-19 by complementing mechanistic models with robust in-sample and out-of-sample predictions. Furthermore, the autoregressive regression framework and RJMCMC method may be applicable to other infectious disease outbreaks characterized by dynamic parameter shifts.

Data availability statement

The COVID-19 data used in this analysis are available in the R-package `COVID19` accessible from CRAN. The data is originally sourced from [COVID-19 Data Hub](#); see [Guidotti \(2022\)](#).

Acknowledgements

I would like to express my sincere gratitude to Dr. Alireza Taheriyoun from The George Washington University for his invaluable guidance to this paper.

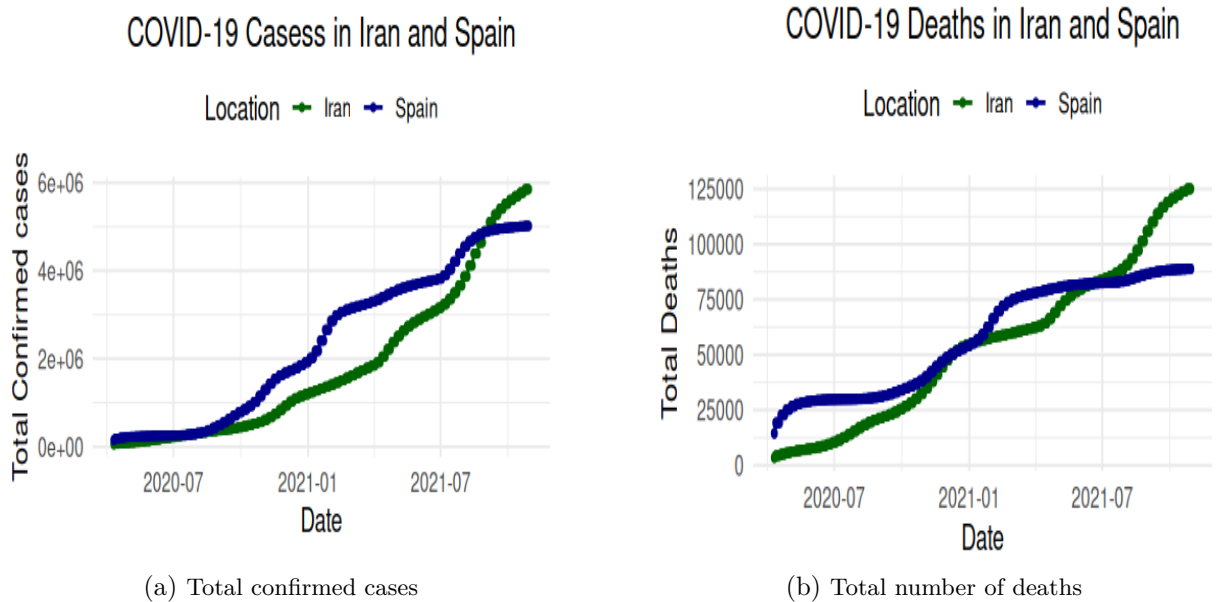


Figure 1: Panel **a**: Total confirmed cases in Iran and Spain from April 10, 2020, to October 30, 2021. Panel **b**: Total deaths in Iran and Spain from April 10, 2020, to October 30, 2021.

References

- Aue, A. and Horváth, L. (2013). Structural breaks in time series. *Journal of Time Series Analysis*, **34**, 1–16.
- Bai, J. (1994). Least squares estimation of a shift in linear processes. *Journal of Time Series Analysis*, **15**, 453–472.
- Bai, J. (1997). Estimation of a change point in multiple regression models. *Review of Economics and Statistics*, **79**, 551–563.
- Bauwens, L., Koop, G., Korobilis, D. and Rombouts, J. V. (2015). The contribution of structural break models to forecasting macroeconomic series. *Journal of Applied Econometrics*, **30**, 596–620.
- Chen, J. and Gupta, A. K. (2011). *Parametric Statistical Change Point Analysis: with Applications to Genetics, Medicine, and Finance*. Springer Science & Business Media.
- Chen, Y. J. Y. and Gu, Y. (2018). Subspace change-point detection: A new model and solution. *IEEE Journal of Selected Topics in Signal Processing*, **6**, 1224–1239.

Algorithm 1 The Proposed RJMCMC Algorithm

Require: $(\xi^{(p,q)}, \alpha^2, k, \varepsilon, k_{max})$ either randomly or deterministically.

0: **for** $i = 1, \dots, \mathcal{T}$ **do**

0: **SM movement-** Update the number and the location of change points with proposed k' and ε' from the proposal densities.

0: $(\xi^{(p,q)}, \alpha^2, k, \varepsilon) \leftarrow (\xi^{(p,q)}^{i-1}, \alpha^{2^{i-1}}, k^{i-1}, \varepsilon^{i-1})$

0: **while** $i \leq N$ **do**

0: Generate k'

0: **if** $k' = k + 1$ **then** {Birth step}

0: Randomly select the segment number s^* to split.

0: Generate ε_{s^*} at random in the s^* th segment and update ε .

0: Update $\alpha^{2'}$ using the appropriate formula.

0: Compute acceptance probability A_1 and generate $v \sim \mathcal{U}(0, 1)$.

0: **if** $A_1 \geq v$ **then**

0: Generate $\xi^{(p,q)'}_{s^*}$, $s = s^*, s^* + 1$, by ARS algorithm.

0: Save $\mathbf{E}' := (\xi^{(p,q)'}, \alpha^{2'}, k', \varepsilon')$ and set $i \leftarrow i + 1$.

0: **else**

0: Go back to select s^* .

0: **end if**

0: **else** [$k' = k - 1$] {Death step}

0: Randomly choose ε_{s^*} and remove it from ε to obtain ε' .

0: $\alpha^{2'}_{s^*} \leftarrow \sqrt{\alpha^2_{s^*} \alpha^2_{s^*+1}}$ and generate $\xi^{(p,q)'}_{s^*}$.

0: Compute acceptance probability A_2 and generate $v \sim \mathcal{U}(0, 1)$.

0: **if** $A_2 \geq v$ **then**

0: Generate $\xi^{(p,q)'}_{s^*}$ by ARS algorithm.

0: Save $\mathbf{E}' := (\xi^{(p,q)'}, \alpha^{2'}, k', \varepsilon')$ and set $i \leftarrow i + 1$.

0: **else**

0: Go back to remove ε_{s^*} .

0: **end if**

0: **end if**

0: **end while**

0: **WM movement-** use the data within each segment to generate the updates $\xi^{(p,q)'}$ and $\alpha^{2'}$.

0: Select one of the change points, ε_{s^*} , and propose a new location for it.

0: Update ε with the new value for ε_{s^*} .

0: Calculate acceptance probability A_3 and generate $v \sim \mathcal{U}(0, 1)$.

0: **if** $A_3 \geq v$ **then**

0: Update α^2 via the Gibbs sampler.

0: Update the coefficients $\xi^{(p,q)}$ using ARS.

0: Save $\mathbf{E} := (\xi^{(p,q)'}, \alpha^{2'}, k', \varepsilon')$.

0: **else**

0: Go back to select a new change point.

0: **end if**

0: **end for**=0

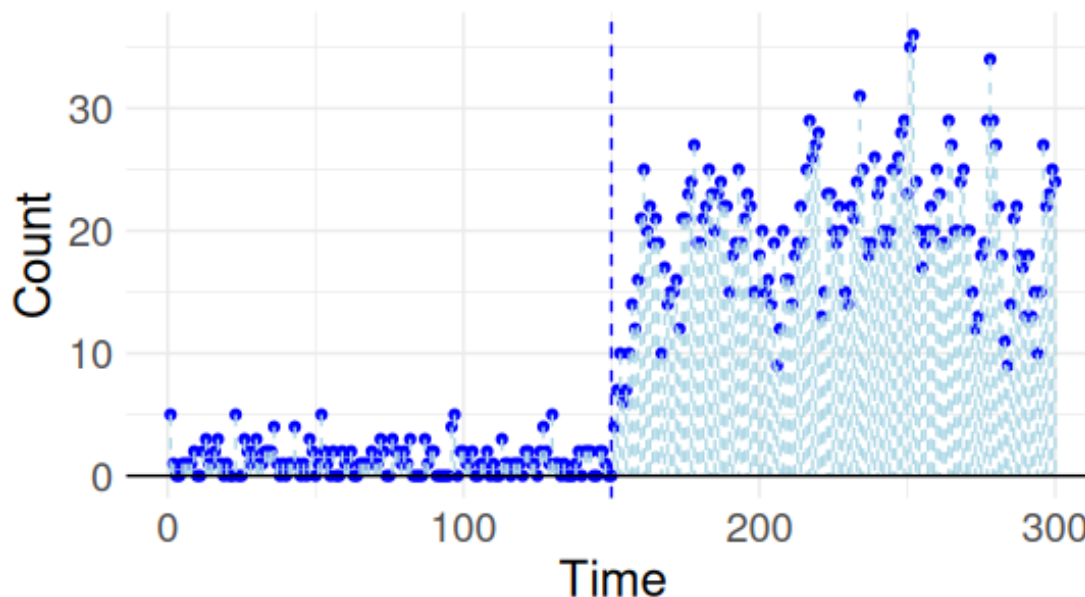


Figure 2: A realization for the dataset 2 in 1.

- Cho, H. and Fryzlewicz, P. (2015). Multiple change-point detection for high-dimensional time series via sparsified binary segmentation. *Journal of the Royal Statistical Society: Series B (Statistical Methodology)*, **77**, 475–507.
- Dehning, J., Zierenberg, J., Spitzner, F. P., Wibral, M., Neto, J. P., Wilczek, M. and Priesemann, V. (2020). Inferring change points in the spread of COVID-19 reveals the effectiveness of interventions. *Science*, **369**, eabb9789.
- Jiang, F., Zhao, Z., and Shao, X. (2023). Time series analysis of COVID-19 infection curve: A change-point perspective. *Journal of Econometrics*, **232**, 1–17.
- Fan, Z. and Mackey, L. (2017). An empirical bayesian analysis of simultaneous changepoints in multiple data sequences. *The Annals of Applied Statistics*, **11**, 2200–2221.
- Fearnhead, P. (2006). Exact and efficient Bayesian inference for multiple changepoint problems. *Statistics and Computing*, **16**, 203–213.
- Fokianos, K. (2012) Count time series models. *Handbook of Statistics*, **30**, 315–347.
- Fryzlewicz, P. (2014). Wild binary segmentation for multiple change-point detection. *The Annals of Statistics*, **42**, 2243–2281.
- Jiang, F., Zhao, Z., and Shao, X. (2022). Modelling the COVID-19 infection trajectory: A piecewise linear quantile trend model. *Journal of the Royal Statistical Society Series B: Statistical Methodology*, **84**, 1589–1607.

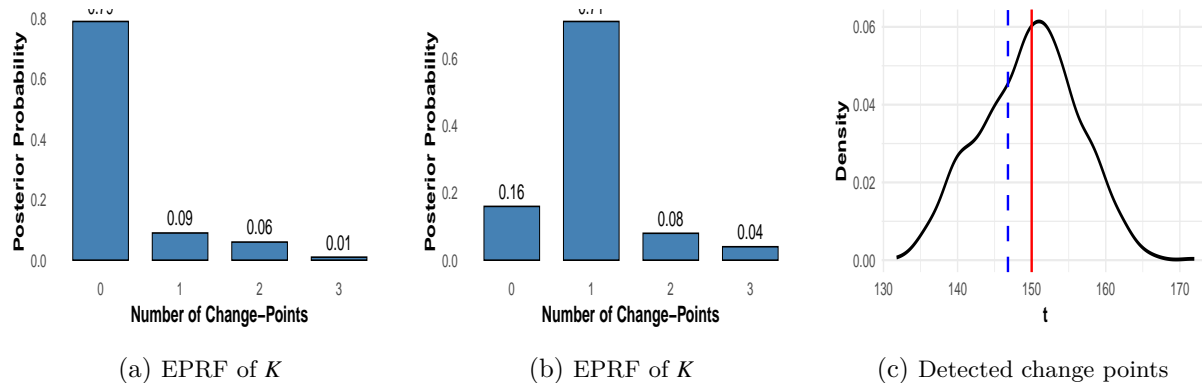


Figure 3: Panel (a) and Panel (b) display the empirical posterior relative frequency (EPRF) of the number of change points, considering $k_{\max} = 4$ and $n_{\min} = 20$, for datasets without and with change points, respectively. Panel (c) illustrates the posterior densities for the location of the change point, where the actual change point and the detected change point are represented by solid and dashed lines, respectively.

- Gilks, W. R and Wild, P. (1992). Adaptive rejection sampling for Gibbs sampling. *Journal of the Royal Statistical Society: Series C (Applied Statistics)*, **41**, 337–348.
- Green, P. J. (1995). Reversible jump Markov chain Monte Carlo computation and Bayesian model determination. *Biometrika*, **82**, 711–732.
- Gromenko, O. and Kokoszka, P. and Reimherr, M. (2017). Detection of change in the spatiotemporal mean function. *Journal of the Royal Statistical Society: Series B (Statistical Methodology)*, **79**, 29–50.
- Guidotti, E. (2022). A worldwide epidemiological database for COVID-19 at fine-grained spatial resolution. *Scientific Data*, **9**, 112.
- Ko, S. I. M. and Chong, T. T. L. and Ghosh, P. (2015). Dirichlet process hidden Markov multiple change-point model, *Bayesian Analysis*, **10**, 275–296.
- Majidizadeh, M. and Taheriyoun, A. R. (2024). Bayesian multiple change-points detection in autocorrelated binary process with application to COVID-19 infection pattern. *Journal of Statistical Computation and Simulation*, **94**, 3723–3749.
- Majidizadeh, M. (2024). Bayesian analysis of the COVID-19 pandemic using a Poisson process with change-points. *Monte Carlo Methods and Applications*, **30**, 449–465.
- Perron, P. (2006). Dealing with structural breaks. *Palgrave Handbook of Econometrics*, **1**, 278–352.
- Pesaran, M. H. and Timmermann, A. (2002). Market timing and return prediction under model instability. *Journal of Empirical Finance*, **9**, 495–510.

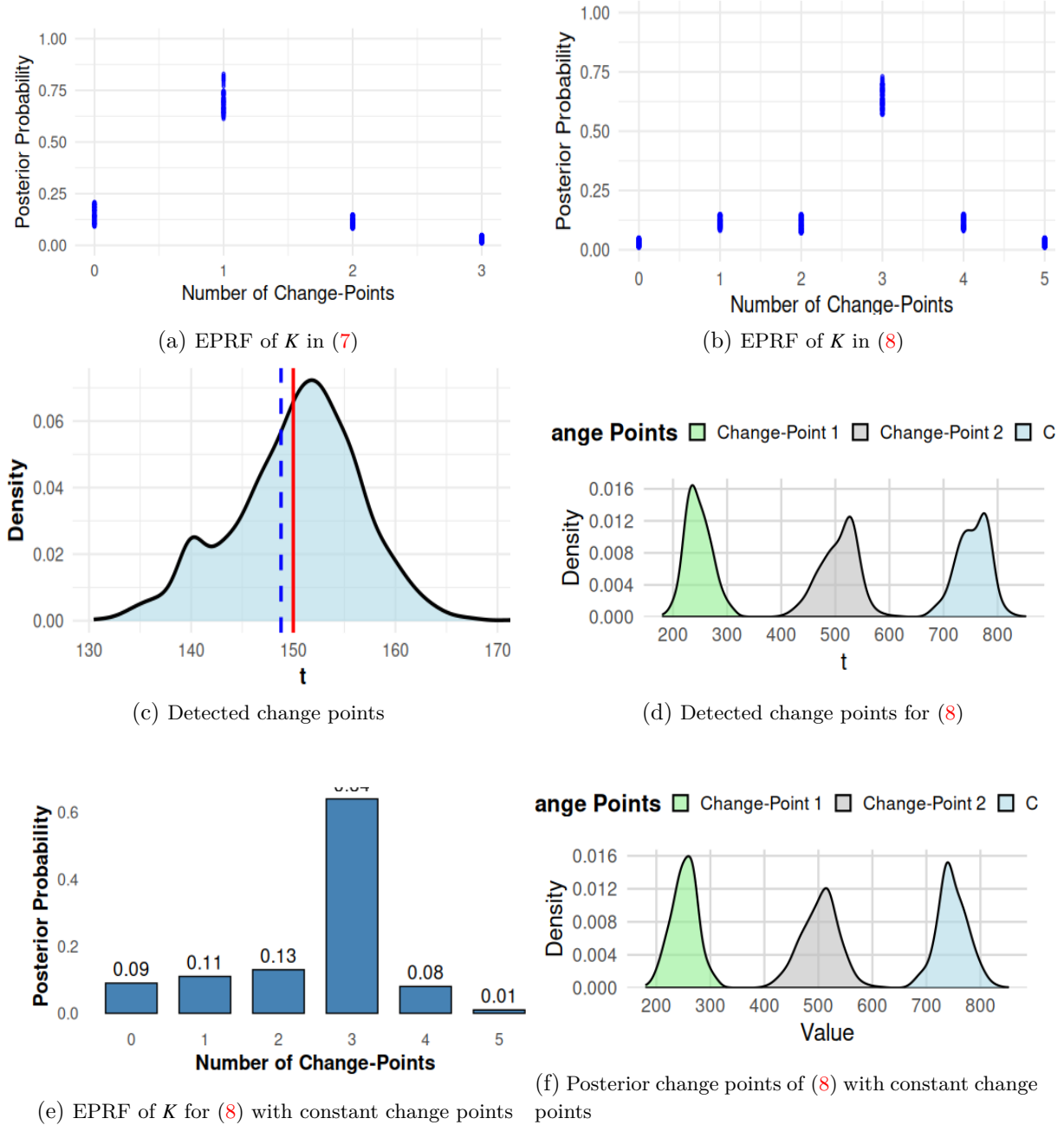
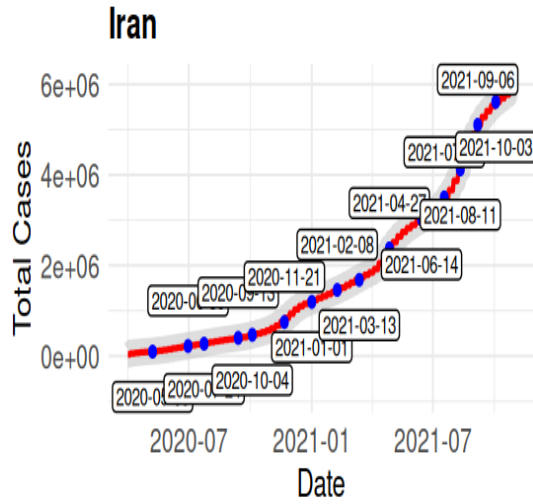
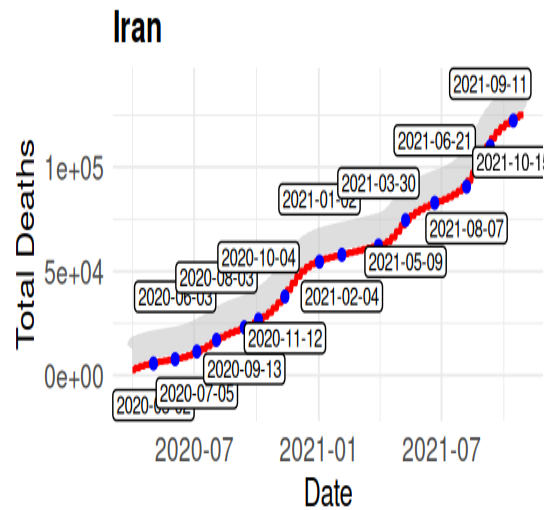


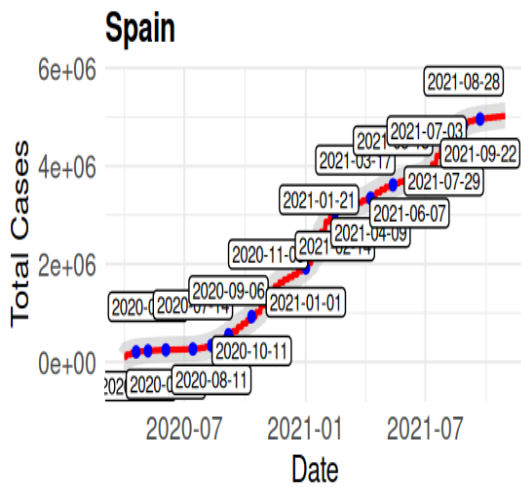
Figure 4: Panels (a), (b), and (e): The estimated posterior frequencies of the number of segments for models (7) and (8), and the fixed change point, respectively. Panels (c), (d), and (f): The posterior densities for the location of the change points regarding to model (7), model (8) with random change points and constant change points, respectively.



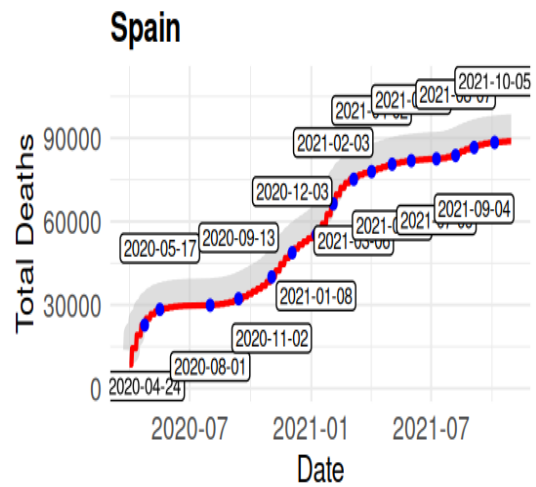
(a) Iran total cases



(b) Iran total deaths



(c) Spain total cases



(d) Spain total deaths

Figure 5: The estimated change point locations, based on the Poisson time series model, indicate changes in the confirmed cases and deaths for the total cases in Iran (see Figure a), total deaths in Iran (see Figure b), confirmed cases in Spain (see Figure c), and total deaths in Spain (see Figure d) from April 10, 2020, to October 30, 2021. The points and dates identified in each plot were determined using parameters $k_{\max} = 20$ and $n_{\min} = 20$.

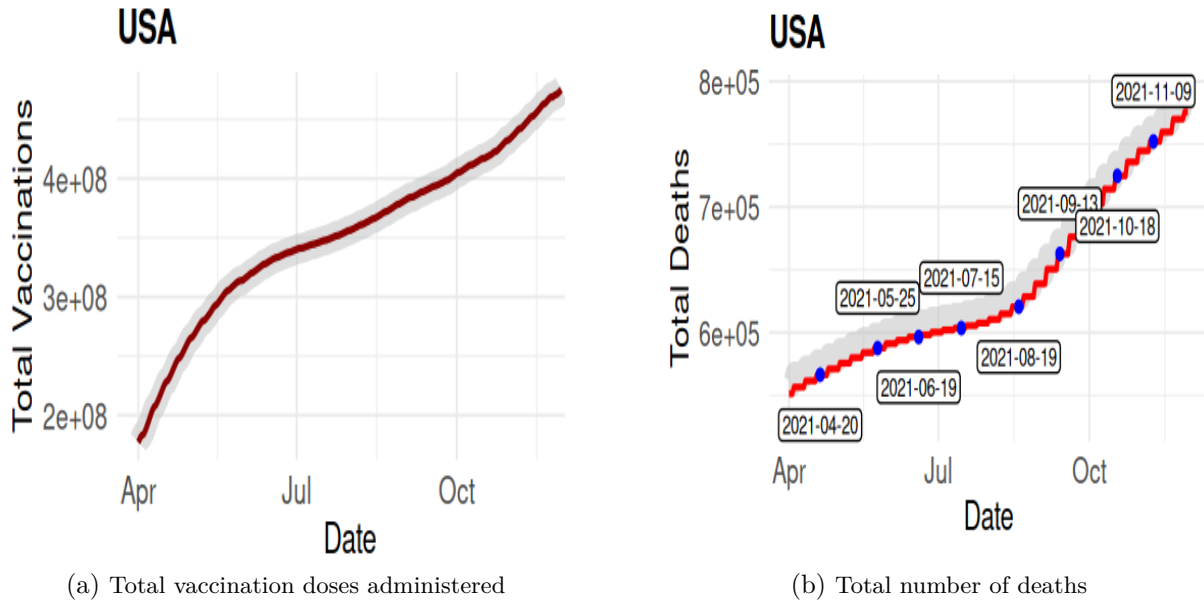


Figure 6: Panel **a**: Total number of vaccine doses administered in the United States from April 1, 2021, to November 30, 2021. Panel **b**: Cumulative number of mortality cases during this period, with labels indicating the detected change points based on the parameters $k_{\max} = 5$ and $n_{\min} = 20$.

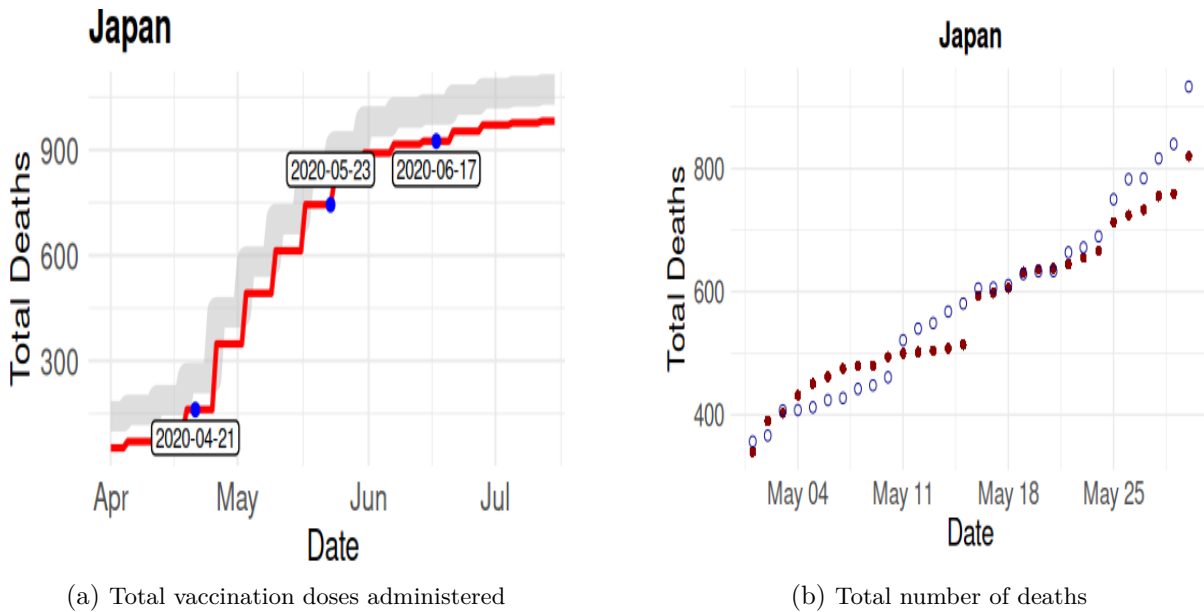


Figure 7: Panel **a**: Total deaths in Japan from April 1, 2020, to July 15, 2020, and detected change points. Panel **b**: Actual (solid points) and forecasted (hollow points) COVID-19 deaths data in Japan from May 1, 2020, to May 30, 2020.

- ST, P. K. and Lahiri, B. and Alvarado, R. (2022). Multiple change point estimation of trends in Covid-19 infections and deaths in India as compared with WHO regions, *Spatial Statistics*, **49**, 100538.
- Truong, C. and Oudre, L. and Vayatis, N. (2020). Selective review of offline change point detection methods. *Signal Processing*, **167**, 107299.
- Zhang, N. R. and Siegmund, D. O. (2007). A modified Bayes information criterion with applications to the analysis of comparative genomic hybridization data. *Biometrics*, **63**, 22–32.
- Wei, C. H. (2018). *An Introduction to Discrete-Valued Time Series*. John Wiley & Sons, New York.

Table 3: Estimations, including standard errors, of the Poisson time series model applied to the COVID-19 deaths dataset in Iran. This analysis utilizes the logarithm of the total administered tests and the total confirmed cases as covariates. The dataset spans from April 10, 2020, to October 30, 2021, and is divided into 17 segments, with five parameters estimated for each segment.

Segment	a	b	c_1	c_2	d
1	-1.0807 (0.5437)	0.7473 (0.2543)	-0.0011 (0.6207)	0.0015 (0.8405)	0.7703 (0.7890)
2	-0.3087 (0.0746)	1.9667 (0.3354)	0.0034 (0.0470)	0.0014 (0.1890)	0.3283 (1.0526)
3	1.1003 (0.3456)	0.6947 (0.7543)	0.0051 (0.9012)	-0.0070 (0.4001)	-1.3630 (0.2342)
4	-1.4946 (1.0276)	2.1091 (0.6002)	-0.0095 (0.3451)	-0.0162(0.0050)	0.4031 (0.0703)
5	0.4769 (0.9205)	1.1886 (1.020)	0.0011 (0.02)	0.0009 (0.4409)	0.3078 (0.5802)
6	-1.4659 (0.2708)	2.3436 (0.0214)	-0.0046 (0.3882)	0.0010 (0.6634)	-0.5215 (1.03)
7	-1.602 (0.3945)	1.0993 (0.8002)	-0.0079 (0.2500)	0.0012 (0.5432)	1.1756 (0.7365)
8	1.3020 (0.3500)	0.3862 (0.2901)	0.0051 (0.6345)	0.0009 (0.0550)	0.3757 (0.9102)
9	0.2840 (0.3756)	1.4862 (1.0452)	0.0019 (0.1987)	0.00103 (0.7432)	-1.3106 (1.0210)
10	0.00109 (0.0324)	0.6483 (0.5278)	0.0099 (0.7000)	0.0009 (0.0264)	-0.0809 (0.4932)
11	0.0777 (0.8008)	1.0347 (0.6543)	0.0032 (0.8765)	0.013 (0.0902)	-1.8303 (0.1456)
12	0.5987 (0.1267)	1.32054 (0.4534)	0.0025 (0.0278)	0.01390 (0.5789)	-1.8617 (0.0334)
13	-0.4265 (0.0524)	0.5533 (0.7500)	-0.8977 (0.3845)	0.0175 (0.8342)	-0.1452 (0.6500)
14	-0.5959 (0.2109)	0.8422 (0.8300)	-0.0076 (0.7654)	0.0120 (0.3098)	1.3942 (0.6457)
15	-1.1527 (0.0950)	2.6188 (0.9987)	-0.0019 (0.4251)	0.0168 (0.1005)	0.4474 (0.2056)
16	1.7230 (0.4789)	0.8007 (0.2505)	0.0014 (0.5987)	0.0084 (0.3054)	-1.4603 (0.6843)
17	-0.4094 (0.02)	2.1373 (0.02)	-0.0021 (0.02)	0.0079 (0.02)	-0.8996 (0.02)

Table 4: Estimations (including standard errors) of the Poisson time series model for the COVID-19 deaths dataset in the USA, utilizing the logarithm of the total number of vaccinated individuals, along with school closures and stay-at-home measures as covariates. The dataset from April 1, 2021, to November 30, 2021, is divided into nine segments, with six parameters estimated for each segment.

Segment	a	b	c_1	c_2	c_3	d
1	0.0012 (0.01)	1.8623 (0.015)	-0.0017 (0.02)	0.0069 (0.025)	-1.1399 (0.03)	-1.2166 (0.035)
2	-0.30231 (0.02)	10.1215 (0.025)	0.00085 (0.03)	-0.0122 (0.035)	-1.1402 (0.04)	-0.0211 (0.045)
3	-0.0071 (0.015)	0.0904 (0.02)	0.00084 (0.025)	0.0017 (0.03)	-1.0756 (0.035)	-0.0199 (0.04)
4	-0.0012 (0.025)	0.0859 (0.03)	0.00083 (0.035)	-1.5203 (0.04)	0.4031 (0.045)	0.0116 (0.05)
5	-0.0246 (0.02)	0.0969 (0.025)	0.00082 (0.03)	-0.0024 (0.035)	-1.5203 (0.04)	-0.0194 (0.045)
6	-0.7692 (0.04)	1.5803 (0.045)	0.00012 (0.05)	-2.2715 (0.055)	-1.5238 (0.06)	0.1145 (0.065)
7	0.0081 (0.02)	1.5522 (0.025)	-0.0079 (0.03)	0.0183 (0.035)	-0.0474 (0.04)	0.9090 (0.045)
8	-0.0010 (0.01)	1.7845 (0.015)	-0.00008 (0.02)	0.1578 (0.025)	0.1582 (0.03)	-0.9739 (0.035)
9	-0.0334 (0.03)	0.0751 (0.035)	0.00016 (0.04)	0.1563 (0.045)	0.1536 (0.05)	-0.01962 (0.055)